CRYSTAL GROWTH & DESIGN

Article

pubs.acs.org/crystal

Charge Density Analysis of 2,6-Dinitrophenol

Simone Cenedese, Vladimir V. Zhurov, and A. Alan Pinkerton*

Department of Chemistry, University of Toledo, Toledo, Ohio 43606, United States

Supporting Information

ABSTRACT: The charge density of 2,6-dinitrophenol has been carefully determined from low temperature (20 K) single crystal X-ray diffraction data and periodic *ab initio* theoretical calculations. The topological analysis performed on the refined densities within the framework of the Quantum Theory of Atoms in Molecules (QTAIM), allowed us to characterize, both qualitatively and quantitatively, the various intra- and intermolecular interactions existing in the crystal structure of this compound. Notably two strong intramolecular noncovalent interactions have been characterized (O···H, D_e > 60 kJ/mol; O···O, D_e ∼ 19 kJ/mol). In addition, a series of weaker intermolecular interactions (O···N, O···O, O···C, and C···C) with estimated dissociation energies of 1−9 kJ/mol have been identified.

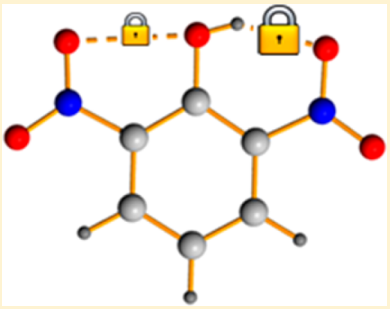

1. INTRODUCTION

It is no novelty that chemical and physical properties of organic crystals are not only a result of the strong interactions defining the molecular structure itself but also depend on the weak noncovalent interactions.[1] Among such interactions, the most famous and well-studied one is with no doubt the hydrogen bond,[2] considered of paramount importance, for example, in protein folding and in biological activity in general. There exists, however, a wealth of other van der Waals interactions that have only recently begun to be studied in a more quantitative way,[3] due to improvements in the accuracy of modern diffractometers and data processing software.[4] The crystal structure of 2,6-dinitrophenol, DNP, (Figure 1) has been known for a long time,[5] and it has been recognized that the two nitro groups ortho to the hydroxyl group could be responsible for hindering free rotation of the latter around the C−O bond.[6] In addition, there is much current interest in the crystal engineering community in understanding the interactions responsible for crystal growth and molecular packing motifs.[7] To the best of our knowledge, no studies addressing a more quantitative description of the nature of the intra- and intermolecular interactions in the crystal of 2,6-dinitrophenol have appeared.

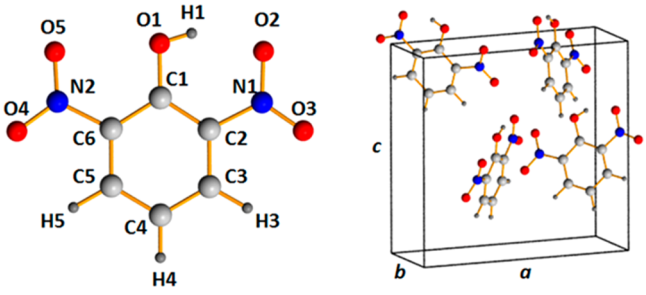

Figure 1. 2,6-Dinitrophenol molecule (left) and unit cell (right). These images, as well as the ones in Figures 5, 6, and 7, were prepared with the Diamond package.[33]

We have carried out a detailed study of the electron density of this molecule, obtained both from an accurate low temperature (20K) X-ray diffraction experiment and periodic ab initio theoretical calculations. In particular, through the topological analysis of these densities, as proposed in the quantum theory of atoms in molecules (QTAIM),[8] we detail here the various inter- and intramolecular interactions characterizing this compound in the solid state. An estimate of their corresponding dissociation energies[9] is also given and discussed.

2. EXPERIMENTAL SECTION

2.1. Data Collection and Reduction. According to the literature, a previous study of this compound was performed on needle shaped crystals obtained from a cyclohexane solution.[5] Following this procedure, however, did not allow us to harvest crystals of suitable quality for a charge density study. Given the aromatic nature of 2,6-dinitrophenol, it was decided to attempt growing crystals by sublimation. DNP powder (purchased from Sigma-Aldrich) was placed in a Pyrex tube and then sealed under vacuum. One end of the tube was kept at 53 °C in a cylindrical heater. After a few days, many well-formed yellow rod-shaped crystals were obtained. While for the major part they were greatly elongated in one direction, we were able to collect a 0.20 × 0.29 × 0.29 mm^3 crystal that proved suitable for a precise diffraction experiment. The crystal was mounted on a nylon loop with KRYTOX lubricant to avoid dissolving in oil and cooled with an open flow He cryostat.[10] The temperature was maintained at 20 K (±0.05) throughout the experiment. The intensity data were collected with a Rigaku rotating anode diffractometer (Ultrax-18 generator, Mo Kα, graphite monochromator, cylindrical image plate RAPID detector) operated at 50 kV, 300 mA power. All together six runs consisting of 71 images each (5° omega scans, 120 s

Received: November 14, 2014
Revised: December 18, 2014
Published: December 19, 2014

DOI: 10.1021/cg5016725
Cryst. Growth Des. 2015, 15, 875−883

accumulation time) were measured at different setting angles (χ = 0; φ = 0, 180; χ = 40; φ = 0, 90, 180, 270°). Consecutive images in each run were overlapped by a half oscillation range. The observed diffraction spots were indexed with HKL2000 software.[11] The obtained reflection positions were then used for integration with the program VIIPP.[4,12] Accumulated background and peak profiles were used during extraction of intensities of fully recorded, nonoverlapped reflections. Resulting peak intensities were scaled and merged with the program SORTAV.[13] The main crystallographic information and refinement details are reported in Table 1.

Table 1. Crystallographic Data and Experimental Details

chemical formula	$C_6H_4N_2O_5$
space group	$Pna2_1$ (#33, orthorhombic)
a (Å)	12.4092(2)
b (Å)	4.6608(1)
c (Å)	11.8316(2)
volume (Å)^3, Z	684.30, 4
T (K)	20.00(5)
wavelength λ (Å)	0.71073 (Mo K_α)
cystal size (mm)	0.20 × 0.29 × 0.29
$(\sin\theta/\lambda)_{max}$ (Å^{-1})	1.3
reflections integrated	84402
R_{int}/average data multiplicity	0.0174/14.5
completeness: sin θ/λ < 1.00 Å^{-1}, all data (%)	96.9, 90.2
independent reflections	5830
observed reflections ($I > 3\sigma$)	5529
Spherical Atom Refinement	
R_1, wR_2, GOF	0.0217, 0.0652, 1.079
$\Delta\rho_{min/max}$ (eÅ^{-3})	−0.26/0.44
Multipole Refinement	
R_1, wR_2, GOF	0.0124, 0.0123, 1.159
weighting scheme: a, b[a]	0.002, 0.002
$\Delta\rho_{min/max}$: all data/sin θ/λ < 1.00 Å^{-1} (eÅ^{-3})	−0.224, 0.118/−0.141, 0.093

[a] $w_2 = 1/\{\sigma^2(F^2) + (ap)^2 + bp\}$, $p = 0.3333F^2_{obs} + 0.6667F^2_{calc}$

2.2. Multipole Refinement of Experimental Structure Factors. The unaveraged data were used to resolve and refine the crystal structure with the SHELXTL program suite.[14] The independent atom model (IAM) from SHELXTL was then used as a starting point for refinement of the experimental charge density over the averaged data using the Hansen−Coppens multipole model[15] as implemented in the program XD2006.[16] Reflections with $I/\sigma(I) > 3$ and sin $\theta/\lambda \leq 1.3$ Å^{-1} were included in the refinement. The VM databank was adopted. In a first model, the atomic positions were refined for all the atoms. For carbon, nitrogen, and oxygen atoms, anisotropic displacement parameters and all of the multipoles up to the hexadecapole level were considered, while isotropic thermal parameters and multipoles up to the quadrupole level were used for the hydrogen atoms. For H3, H4, and H5 only the first quadrupole (Q0, bond directed) was considered; however, it proved necessary to refine all quadrupoles for H1 to obtain a satisfactory result. Both κ and κ', the variables governing the expansion/contraction of the spherical and aspherical valence density, have been refined for the heavy atoms (constraining κ' to the same value for all the multipoles of the same atom) and kept fixed to the suggested value of 1.2 for H atoms.[17] In addition, an isotropic type-1 extinction correction with a Lorentzian mosaic distribution was performed. Finally, all parameters were corefined to ensure proper convergence.

Despite the proposed model looking satisfactory, an *a posteriori* evaluation, based also on the results obtained from the topological analysis, made us reconsider some of the steps undertaken in the refinement. In particular, a major concern was the rather short distance d(O1−H1) = 0.8191 Å obtained from the refinement. Unfortunately, no neutron d(O−H) bond distance is available for this particular compound, yet the vast majority of d(O−H) bond lengths reported for neutron studies on phenolic compounds fall within the 0.98−1.00 Å range.[18] We thus decided to optimize the d(O1−H1) distance by means of ab initio calculations (vide infra) and then keep it fixed while performing the multipole refinements. The optimization was carried out on H1 coordinates only and, as a further check to ensure there is no other minimum along the O1−H1 interaction line, starting both from 0.8191 Å (experimental) and 1.225 Å (arbitrary) d(O1−H1) values. In both cases, within numerical accuracy, the optimized bonding distance was found to be d(O1−H1) = 0.9906 Å. A new refinement was then performed, constraining d(O1−H1) to this value while adjusting all other structural parameters. The same multipoles discussed above were included in the refinement of carbon, nitrogen, and oxygen atoms, while only the bond directed dipole and quadrupole were considered for each hydrogen atom. As before, κ and κ' were refined for the heavy atoms, while keeping κ and κ' set to 1.2 for hydrogens. Finally, all of the parameters were refined together to ensure proper convergence. The resulting model, labeled MM_{exp} in the following, was adopted for the charge density analysis.

Even though no symmetry constraints have been imposed during the refinement, the deformation density maps (Figure 2) highlight features that, given the molecular structure, are expected to show a significant degree of symmetry. In particular, the lone pairs around the oxygen atoms are symmetrically placed with respect to the N−O bonds. The residual density map (Figure 3) shows no "structured" features, as expected from a reliable refinement.

2.3. Computational Details. The theoretical charge density has been obtained by performing periodic *ab initio* DFT calculations employing the program CRYSTAL09.[19] The B3LYP functional[20] was used with the standard 6-311G** basis sets for H and N atoms and slightly modified ones for C and O.[21]

A preliminary single point energy calculation was performed with the unit cell and atomic positions fixed to the values obtained from the first multipole refinement. This was used as a starting point for the optimization of the d(O1−H1) bonding distance described above. Following refinement of the MM_{exp} model described above, another single point energy calculation was performed. The charge density analysis based on the obtained wave function, labeled *theo* in the following, was performed with the program TOPOND.[22] In addition, static theoretical structure factors were calculated up to the experimental sin θ/λ and a multipole refinement performed on the charge density reconstructed from these theoretical structure factors

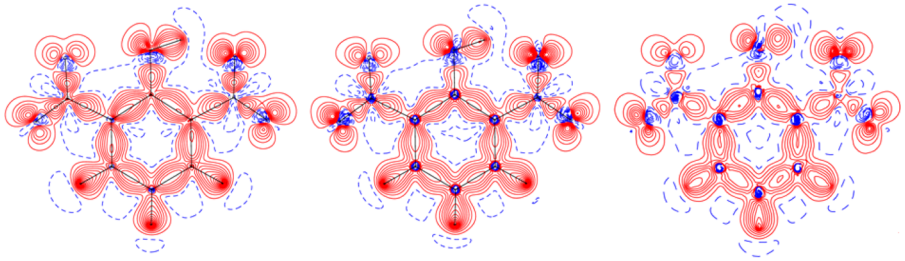

Figure 2. Static deformation density maps: MM_{exp} (left), MM_{theo} (middle), and *theo* (right). Contour levels are drawn at 0.1 eÅ^{-3}. Orientation and atom labels correspond to Figure 1

DOI: 10.1021/cg5016725
Cryst. Growth Des. 2015, 15, 875−883

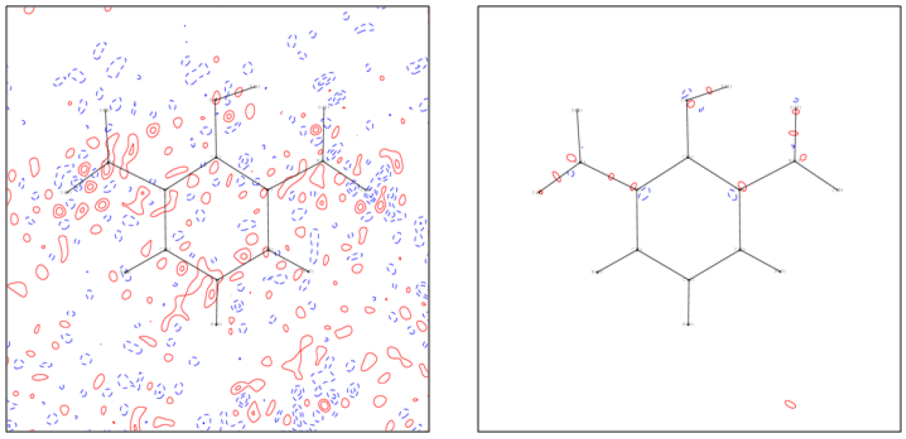

Figure 3. Residual maps: MM_{exp} (left) and MM_{theo} (right). Contour levels are drawn at 0.05 eÅ^{-3}.

(MM_{theo}). To effectively describe the charge density features, in particular in the region close to the heavy atom nuclei, a second spherical valence term, P_{00}, with an appropriate κ_0 accounting for its expansion/contraction, has been added to the traditional P_v and κ_s variables for each non-hydrogen atom.[3b,23] In addition, in contrast to MM_{exp}, all κ' parameters were refined separately for each order of multipole without imposing constraints. However, hexadecapoles were only considered for O atoms as they were found to be negligibly occupied for the carbon and nitrogen atoms. All dipoles and the bond directed quadrupole were used to describe the hydrogen atoms. In the final cycles, all of the parameters were refined simultaneously to ensure proper convergence.

The static deformation density map shows features similar to the ones obtained from MM_{exp} (Figure 2). As expected,[3b,23] the introduction of the additional monopole term, P_{00}, in the refinement leads to a residual density map with no significant features (Figure 3).

3. RESULTS AND DISCUSSION

3.1. Covalent Interactions. The total electron densities obtained from the multipole refinements, MM_{exp} and MM_{theo}, and from theoretical calculations, *theo*, have been analyzed within the framework of the QTAIM.[8] The program WinXPro[24] was used for the first two, while TOPOND[22] was adopted for the latter.

One of the cornerstones of QTAIM is that two atoms are considered to be chemically bonded if there exists a (3,−1) bond critical point (bcp) in the electron density (ρ) between them, and the bond path connecting them should be mirrored by a virial path in the negative potential energy density linking the same attractors. In Tables 2 and 3, the main topological descriptors for DNP intra- and intermolecular interactions, respectively, are reported. For the bonds in the aromatic ring, very good agreement is found between all three models. The small differences in C−C bond lengths are expected for substituted aromatic rings, and the Laplacian ($\nabla^2\rho$) values at the bcps are close to the ones reported for benzene.[25]

The two nitro groups are both slightly off plane with respect to the aromatic ring (C1−C2−N1−O2 = −2.3°; C1−C6−N2−O5 = 11.7°). For the various models, the C−N and N−O Laplacian values at the bcp are close to the ones found for the C−C interactions, suggesting an increased delocalized system encompassing not only the ring but also these substituents. However, the topological bond orders, n_{topo} (Table 2),[26] are closer to 1 for the C−N and to 2 for the N−O interactions, revealing how this charge redistribution is only partial. Moreover, as will be discussed in more detail later, the nitro groups lie close to the aromatic ring plane. We believe this to be a consequence of the intra- and intermolecular interactions developed in the crystal rather than any inherent restriction to rotation around the C−N bonds.

The difference in $\nabla^2\rho$ values between MM_{exp} and *theo* can be in part related to the different positions of the bcp as can be seen in Figure 4. The Laplacian profiles also reveal that a more pronounced charge separation is found for MM_{exp}, even though the negative sign of $\nabla^2\rho$ still identifies these as shared shell interactions. For *theo*, however, the O and N valence shell charge concentrations show almost the same value. In the case of MM_{theo}, however, it can be seen that the bias between experiment and theory is reduced and that $\nabla^2\rho$ values closer to MM_{exp} are found, as is also true for the C1−O1 and O1−H1 interactions (Figure 4).

3.2. Intramolecular Noncovalent Interactions. The description of the molecular structure of DNP would not be complete without addressing the two intramolecular interactions listed at the bottom of Table 2, and shown in Figure 5. The O1−H1···O2 hydrogen bond was, not surprisingly, already addressed as one of the prominent features of this molecule. In particular, on the basis of dielectric absorption studies,[6] it was suggested that the barrier to rotation of the OH group around the C−O bond is strongly dependent on the energy required to break the hydrogen bond. We are now in a position to address this more quantitatively. The positive value of the Laplacian at the bcp (Table 2) identifies this as a closed shell interaction, as expected. However, taking into account the ratio between the potential, V_{bcp}, and kinetic, G_{bcp}, electronic energy densities evaluated at the bcp,[27,28] we found $|V_{bcp}|/G_{bcp}$ = 0.98, 1.14, and 1.19, respectively, for MM_{exp}, MM_{theo}, and *theo*, and the corresponding total electronic energy density $H_{bcp} = V_{bcp} + G_{bcp}$ is slightly positive for MM_{exp} (2.18 kJ/mol) and negative for MM_{theo} and *theo* (−16.39 kJ/mol and −22.84 kJ/mol). According to the $|V_{bcp}|/G_{bcp}$ criterion,[28] our experimental model still identifies this H-bond as a closed shell interaction but close to the boundary of what has been termed the "transit region" for covalent bond formation, for which $1 < |V_{bcp}|/G_{bcp} < 2$. It is then not surprising that the estimated[9] dissociation energy D_e of the O1−H1···O2 hydrogen bond is found to be above 60 kJ/mol (D_e = 60.73 kJ/mol, 65.72 kJ/mol, and 70.63 kJ/mol, respectively, for MM_{exp}, MM_{theo}, and *theo*), quantitatively supporting the idea that a high energy barrier should be overcome in order to break this bond.

However, this is only part of the total picture as the other intramolecular interaction, O1···O5, also has a non-negligible

DOI: 10.1021/cg5016725
Cryst. Growth Des. 2015, 15, 875−883

Table 2. Topological Parameters for the Intramolecular Bond Critical Points[a]

bond	d (Å)	ρ (eÅ^{-3})	$\nabla^2\rho$ (eÅ^{-5})	λ_1 (eÅ^{-5})	λ_2 (eÅ^{-5})	λ_3 (eÅ^{-5})	ε	n_{topo}
C1−C2	1.4178	2.041	−16.11	−15.82	−12.97	12.68	0.22	1.27
		2.002	−16.51	−15.16	−11.94	10.59	0.27	1.31
		2.021	−18.53	−15.78	−12.59	9.84	0.25	1.19
C2−C3	1.3956	2.111	−18.04	−16.47	−14.05	12.48	0.17	1.24
		2.045	−17.50	−15.41	−12.49	10.40	0.23	1.33
		2.083	−19.81	−15.92	−13.37	9.48	0.19	1.24
C3−C4	1.3852	2.133	−19.44	−16.72	−14.07	11.34	0.19	1.24
		2.097	−18.16	−15.54	−13.01	10.39	0.19	1.39
		2.123	−20.60	−16.28	−13.77	9.45	0.18	1.25
C4−C5	1.3919	2.085	−19.08	−16.04	−14.11	11.07	0.14	1.18
		2.088	−17.85	−15.42	−12.99	10.57	0.19	1.38
		2.097	−20.18	−16.00	−13.68	9.50	0.17	1.23
C5−C6	1.3917	2.121	−18.72	−16.90	−14.00	12.18	0.21	1.22
		2.103	−18.18	−15.76	−12.82	10.39	0.23	1.40
		2.102	−20.09	−16.15	−13.43	9.48	0.20	1.25
C6−C1	1.4166	2.076	−17.36	−16.67	−13.28	12.59	0.25	1.22
		2.012	−16.83	−15.52	−11.98	10.67	0.30	1.30
		2.026	−18.79	−15.94	−12.69	9.84	0.26	1.18
C3−H3	1.0600	1.913	−20.00	−18.38	−17.79	16.17	0.03	0.99
		1.969	−21.83	−19.15	−18.71	16.02	0.02	0.98
		2.038	−26.68	−21.00	−20.95	15.28	0.00	0.88
C4−H4	1.0337	1.873	−18.99	−17.96	−17.19	16.16	0.04	0.98
		2.085	−24.50	−20.63	−19.70	15.83	0.05	1.02
		2.151	−29.58	−22.68	−22.35	15.45	0.01	0.90
C5−H5	1.0636	1.887	−19.78	−18.01	−17.14	15.38	0.05	0.98
		1.946	−21.10	−18.85	−18.41	16.16	0.02	0.98
		2.022	−26.24	−20.74	−20.70	15.20	0.00	0.88
C1−O1	1.3280	2.325	−25.80	−20.66	−18.54	13.40	0.11	1.19
		2.155	−18.98	−17.30	−15.89	14.22	0.09	1.11
		2.154	−18.57	−17.89	−16.70	16.02	0.07	1.06
O1−H1	0.9906	2.336	−38.69	−37.90	−37.24	36.44	0.02	0.10
		2.257	−40.45	−36.47	−35.85	31.86	0.02	0.27
		2.204	−53.10	−39.51	−38.95	25.37	0.01	0.59
C2−N1	1.4500	1.875	−14.77	−14.41	−12.87	12.51	0.12	0.83
		1.769	−10.95	−13.10	−10.39	12.54	0.26	0.81
		1.811	−17.23	−13.88	−11.54	8.19	0.20	0.77
N1−O2	1.2428	3.242	−11.00	−29.94	−27.79	46.73	0.08	1.81
		3.133	−12.97	−27.95	−25.00	39.99	0.12	1.67
		3.187	−21.37	−30.44	−27.09	36.17	0.12	1.55
N1−O3	1.2203	3.381	−13.33	−31.10	−29.65	47.43	0.05	1.88
		3.324	−16.98	−30.27	−27.19	40.49	0.11	1.75
		3.368	−24.78	−32.23	−28.99	36.44	0.11	1.63
C6−N2	1.4658	1.790	−13.68	−13.47	−11.99	11.78	0.12	0.77
		1.700	−10.05	−12.78	−10.10	12.83	0.27	0.75
		1.774	−16.64	−13.68	−11.65	8.68	0.17	0.73
N2−O4	1.2296	3.306	−9.31	−29.71	−27.76	48.15	0.07	1.90
		3.240	−14.62	−28.96	−26.18	40.53	0.11	1.73
		3.290	−22.95	−31.29	−28.13	36.48	0.11	1.60
N2−O5	1.2248	3.384	−13.59	−31.28	−29.79	47.48	0.05	1.88
		3.284	−16.00	−29.73	−26.63	40.36	0.12	1.74
		3.328	−23.88	−31.80	−28.51	36.44	0.12	1.62
O2···H1	1.6718	0.290	4.62	−2.00	−1.60	8.22	0.25	-
		0.330	3.62	−2.28	−1.94	7.85	0.18	-
		0.352	3.53	−2.22	−2.19	7.93	0.01	-
O5···O1	2.5878	0.126	2.04	−0.44	−0.38	2.86	0.16	-
		0.130	1.85	−0.52	−0.48	2.86	0.07	-
		0.120	2.00	−0.42	−0.41	2.82	0.02	-

[a]For each interaction, the first, second, and third lines refer to the MM_{exp}, MM_{theo}, and *theo* models, respectively. d, bonding distance; ρ, electron density; $\nabla^2\rho$, Laplacian; λ_i (i = 1−3), eigenvalues of the Hessian matrix; ε, ellipticity; $n_{topo,}$ topological bond order.

DOI: 10.1021/cg5016725
Cryst. Growth Des. 2015, 15, 875−883

Table 3. Topological Parameters for the Intermolecular Bond Critical Points[a]

bond	d (Å)	ρ (eÅ^{-3})	$\nabla^2\rho$ (eÅ^{-5})	λ_1 (eÅ^{-5})	λ_2 (eÅ^{-5})	λ_3 (eÅ^{-5})	ε	D_e (kJ/mol)
O3···N2[b]	2.7865	0.081	1.05	−0.22	−0.13	1.40	0.65	9.46
		0.048	1.06	−0.15	−0.05	1.26	1.90	6.80
		0.058	1.12	−0.16	−0.09	1.37	0.72	8.01
O2···O4[c]	2.8544	0.063	0.87	−0.20	−0.14	1.21	0.38	7.12
		0.056	0.89	−0.16	−0.10	1.14	0.70	6.57
		0.054	0.93	−0.16	−0.11	1.20	0.43	6.70
O5···N1[d] (*O5···O3[d]*)†	3.1310 (*3.1427*)	0.046	0.59	−0.13	−0.06	0.77	1.31	4.52
		0.037	*0.58*	*−0.12*	*−0.10*	*0.79*	*0.21*	3.94
		0.040	*0.59*	*−0.12*	*−0.05*	*0.76*	*1.36*	*4.20*
O1···O3[e]	3.1838	0.048	0.59	−0.09	−0.03	0.72	1.74	4.64
		0.037	0.54	−0.10	−0.03	0.67	2.38	3.76
		0.038	0.58	−0.09	−0.05	0.72	0.94	4.07
O5···C1[e] (*O5···C2[e]*)†	3.0485 (*3.0961*)	0.068	0.76	−0.16	−0.05	0.97	2.60	6.96
		0.063	*0.74*	*−0.17*	*−0.09*	*1.00*	*0.96*	*6.48*
		0.057	*0.75*	*−0.16*	*−0.06*	*0.96*	*1.77*	*6.30*
O2···C4[f]	3.1104	0.048	0.53	−0.11	−0.09	0.73	0.18	4.43
		0.040	0.56	−0.09	−0.06	0.71	0.59	4.04
		0.044	0.56	−0.10	−0.08	0.75	0.32	4.46
O4···C3[d] (*O4···C2[d]*)†	3.1580 (*3.3134*)	0.046	0.53	−0.11	−0.05	0.69	1.26	4.27
		0.041	*0.50*	*−0.10*	*−0.06*	*0.66*	*0.56*	*3.79*
		0.044	0.54	−0.11	−0.05	0.70	1.31	3.94
O3···H4[g]	2.4246	0.058	0.92	−0.19	−0.18	1.29	0.04	6.90
		0.069	0.77	−0.27	−0.25	1.28	0.08	7.14
		0.065	0.81	−0.23	−0.23	1.27	0.02	7.22
O5···H4[h]	2.5983	0.048	0.68	−0.13	−0.13	0.93	0.02	5.06
		0.041	0.66	−0.12	−0.08	0.87	0.39	4.56
		0.043	0.60	−0.12	−0.12	0.84	0.04	4.20
O2···H3[g]	2.6697	0.037	0.55	−0.10	−0.10	0.75	0.03	3.76
		0.035	0.55	−0.11	−0.06	0.72	0.83	3.71
		0.039	0.51	−0.12	−0.11	0.75	0.09	3.81
O5···H5[h]	2.7472	0.036	0.50	−0.08	−0.07	0.64	0.27	3.48
		0.030	0.50	−0.07	−0.06	0.63	0.29	3.19
		0.031	0.48	−0.08	−0.07	0.64	0.21	3.28
O1···H4[h]	2.8021	0.042	0.52	−0.10	−0.08	0.70	0.25	3.94
		0.036	0.54	−0.09	−0.07	0.70	0.40	3.68
		0.034	0.49	−0.09	−0.06	0.64	0.43	3.28
O1···H5[h]	2.8855	0.037	0.45	−0.08	−0.04	0.58	0.86	3.32
		0.015	0.22	−0.04	−0.03	0.28	0.19	1.28
		0.029	0.44	−0.07	−0.03	0.54	1.64	2.76
C3···C6[i]	3.2711	0.054	0.47	−0.08	−0.01	0.57	6.69	4.54
		0.039	0.45	−0.05	−0.04	0.54	0.30	3.47
		0.046	0.47	−0.07	−0.07	0.61	0.13	4.07

[a]For each interaction, the first, second, and third lines refers to the MM_{exp}, MM_{theo}, and *theo* models, respectively (†: see text). d, bonding distance; ρ, electron density; $\nabla^2\rho$, Laplacian; λ_i (i = 1−3), eigenvalues of the Hessian matrix; ε, ellipticity; D_e, estimated bond dissociation energy.[9] [b]$x - 1/2, -y + 3/2, z$. [c]$-x + 1/2, y + 1/2, z + 1/2$. [d]$x + 1/2, -y + 1/2, z$. [e]$x, y - 1, z$. [f]$-x, -y + 1, z + 1/2$. [g]$-x, -y + 2, z + 1/2$. [h]$-x + 1/2, y - 1/2, z + 1/2$. [i]$x, y + 1, z$.

effect. In this case, no matter the considered topological descriptor, this interaction is found to be closed-shell. The Laplacian at the bcp is always positive (Table 2) and $|V_{bcp}|/G_{bcp}$ = 0.8 for all of the models, and nearly 20 kJ/mol of stabilization is estimated[9,29] to be provided by this bond (D_e = 19.18, 18.87, and 18.38 kJ/mol, respectively, for MM_{exp}, MM_{theo}, and *theo*).

In an attempt to determine whether the strength of the two intramolecular interactions is due to crystal field effects, we performed two additional calculations: the first one on the isolated molecule "cut out" from the crystal (i.e., at the experimental geometry) and a second one on its optimized structure (the computational parameters are the same as detailed in section 2.3). In the first case, the topological parameters evaluated at the O2···H1 and O5···O1 bcps are identical to those reported (Table 2) for *theo*. The optimized structure obtained is in good agreement with ones previously obtained for various other levels of theory,[30] and it must be noted that the nitro group not involved in the H-bond is significantly more out of plane than in the crystal (C1−C6−N2−O5 = 35.0 vs 11.7°). As a consequence, the O5···O1 interaction distance is slightly larger, d(O5−O1) = 2.6950 vs 2.5878 Å. However, both d(O1−H1) and d(O2···H1) were found to be slightly shorter at 0.9893 vs 0.9906 Å and 1.6630 vs 1.6718 Å, respectively. The topological parameters evaluated at the O2···H1 and O5···O1 bcps are barely affected by these geometrical differences, yielding estimated dissociation energies

DOI: 10.1021/cg5016725
Cryst. Growth Des. 2015, 15, 875−883

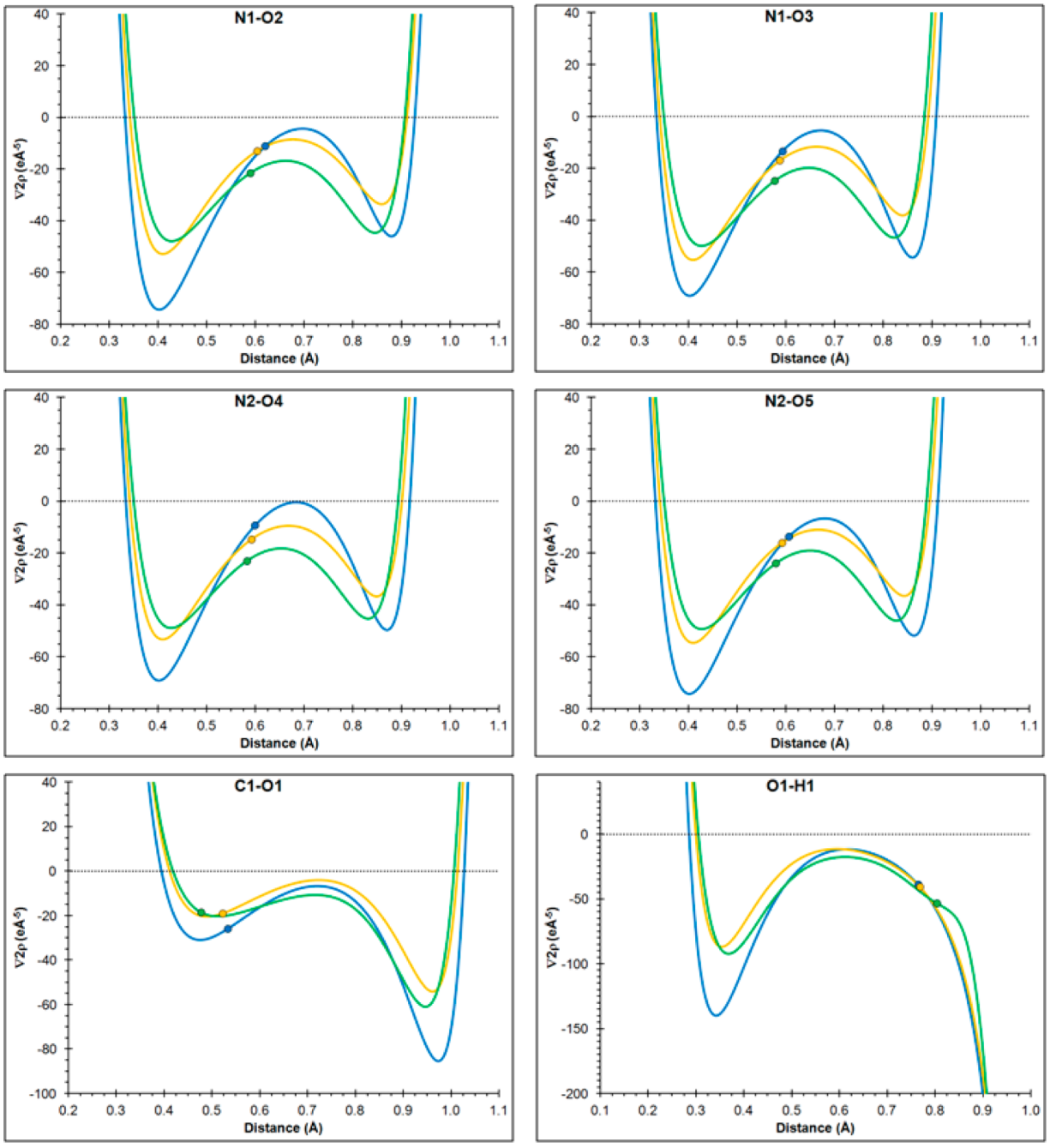

Figure 4. Laplacian profiles along various bonding interactions. Blue, yellow, and green lines refer to MM_{exp}, MM_{theo}, and *theo* models, respectively. The corresponding dots mark the position of the bcp.

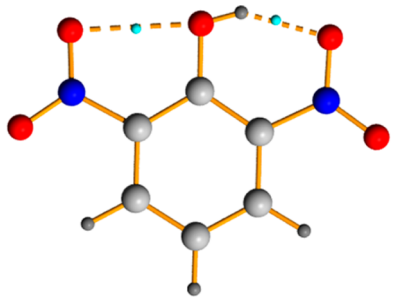

Figure 5. H1···O2 and O5···O1 intramolecular interactions. The light blue sphere represents the bcp position.

of 72.78 vs 70.63 kJ/mol and 13.69 vs 18.38 kJ/mol for the two interactions, respectively. These values are close to the ones found experimentally for the DNP crystal. However, even though rather small, the energy difference for O5···O1 raises the question of whether this interaction alone is responsible for a more planar structure in the crystal or if there are additional contributions. Indeed, the difference of 11.7° vs 35.0° should in principle imply a more significant gap for the D_e values. To clarify this point, it is possible to consider the isolated molecule at the same geometry as in the crystal, thus "switching off" additional contributions from neighboring molecules. The value of D_e = 18.14 kJ/mol found for the O5···O1 interaction is then almost the same as that for the crystal as anticipated. Thus, there is only a minor influence on the energetics of the

DOI: 10.1021/cg5016725
Cryst. Growth Des. 2015, 15, 875−883

intramolecular interactions. We thus conclude that the crystal field mainly affects the molecular geometry, making DNP more planar through the impact of the other weak interactions in which O5 is involved (Table 3). Hence, for the hydroxyl and nitro groups to rotate around the C1−O1 and C−N bonds, respectively, both of these intramolecular interactions have to be broken whether the molecule is embedded in its crystal matrix or "free" in the gas phase.

An additional remark must be made, especially in relation to the atomic charges reported in Table 4, and in particular the value, q(H1) = +0.6, found for the phenolic hydrogen. This value is not surprising, considering that DNP is characterized by a value of pK_a = 3.97. It would be thus reasonable to imagine H1 being "trapped" midway between O1 and O2. However, no evidence supporting this idea was found, either from the refinement of the experimental data or from the optimization of the molecular structure. There is a clear distinction between the O1−H1 and O2···H1 interactions, the former being a (highly) polarized covalent bond and the latter a closed shell interaction. While the positive charge on H1 might have an effect in determining the strength of the H-bond, it has little effect on the electron population of O2, which is identical to that of the other nitro group oxygens.

Table 4. Integrated Atomic Properties

atom	q (e)	V (Å^3)	atom	q (e)	V (Å^3)
O1	−1.09	16.34	C3	0.16	10.00
	−0.95	15.96		0.07	10.38
	−1.12	16.23		0.03	10.32
O2	−0.42	15.85	C4	0.22	10.45
	−0.48	16.10		0.04	11.03
	−0.51	16.35		0.04	10.91
O3	−0.44	15.18	C5	0.19	11.01
	−0.44	15.62		−0.02	11.36
	−0.49	15.69		0.04	11.26
O4	−0.44	15.95	C6	0.21	9.37
	−0.46	16.26		0.17	9.46
	−0.49	16.36		0.24	9.22
O5	−0.42	14.79	H1	0.61	1.52
	−0.46	15.19		0.62	1.53
	−0.48	15.30		0.67	1.29
N1	0.28	7.46	H3	0.06	6.53
	0.39	6.79		0.10	6.32
	0.40	7.00		0.12	6.20
N2	0.27	6.93	H4	0.01	6.44
	0.39	6.56		0.09	5.53
	0.42	6.58		0.10	5.61
C1	0.60	7.52	H5	0.05	6.46
	0.60	7.42		0.13	6.23
	0.65	7.36		0.11	6.29
C2	0.17	9.15			
	0.21	9.12			
	0.26	8.93			

3.3. Intermolecular Noncovalent Interactions. In addition to their impact on the (almost) planar structure of DNP, the two nitro groups are also responsible for the net of intermolecular interactions (Table 3) constituting the crystal. They are all closed-shell in nature, and the estimated dissociation energies are below 10 kJ/mol in all cases. Some of them are responsible for particular geometrical structural features and are discussed in further detail. Considering the dissociation energy values as the reference, the single strongest interaction develops between the $-NO_2$ substituents on neighboring molecules, in particular between O3 and N2. We note that the estimated D_e is similar to what was previously found for N−O interactions in the high energy material RDX.[31] From a geometrical point of view, it can be seen in Figure 6 that this interaction is responsible for a sawtooth-like chain structure along the crystallographic *a* axis.

In order to better understand how this specific configuration arises, we analyzed more closely the topology of the Laplacian in order to highlight points of charge accumulation and charge depletion within the valence shell charge concentration (VSCC) region of the various atoms. Regions of charge accumulation identified by the presence of (3,−3) critical points are commonly referred to as either bonded (BM) or nonbonded maxima (NBM). The former develop when the formation of a bond causes a significant deformation in the VSCC (with respect to the perfectly spherical shape in the isolated atoms) between two bonded atoms; they can be observed in Figure 6 for the N1−O3 bond. The latter identify regions mainly related to charge redistribution within the VSCC of an atom due, for example, to a particular geometrical configuration or hybridization. This is the case of the oxygen atom lone pairs. Clearly, they can have a role in bonding: for example, when (strong) hydrogen bonds are considered, it is expected that the oxygen lone pairs point at the "hole", a (3,+3) critical point, in the VSCC of the hydrogen atom. This is indeed what we find for the O2···H1 interaction. However, the geometrical position and number of NBM are mainly determined not by the onset of intermolecular interactions but rather related to the atom's hybridization. As such, other critical points must be considered when discussing intermolecular interactions. For example, it was found that the (3,−1) critical points of the oxygen atom VSCC are the ones mainly involved in the O···H hydrogen bonds in urea crystals.[32]

In DNP, for O3 we found a situation similar to that reported for urea, with the presence of two (3,−1) critical points lying above and below the O2−N1−O3 plane and whose attractors are the NBM (Figure 6). None of these, however, points

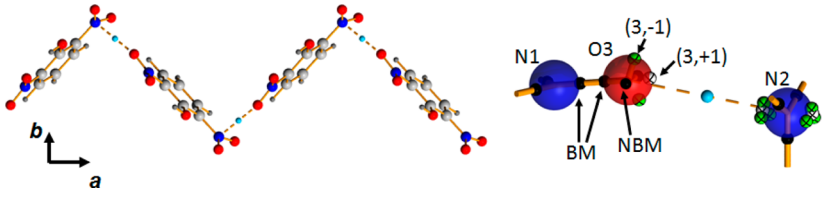

Figure 6. O3···N2 intermolecular interaction. Left, the sawtooth-like structure is highlighted; right, close-up of the interaction highlighting the (3,−3), (3,−1), and (3,+1) Laplacian critical points (black, green, and white small spheres, respectively). For the sake of clarity, only the critical points relevant for this interaction are shown in this image (see text).

DOI: 10.1021/cg5016725
Cryst. Growth Des. 2015, 15, 875−883

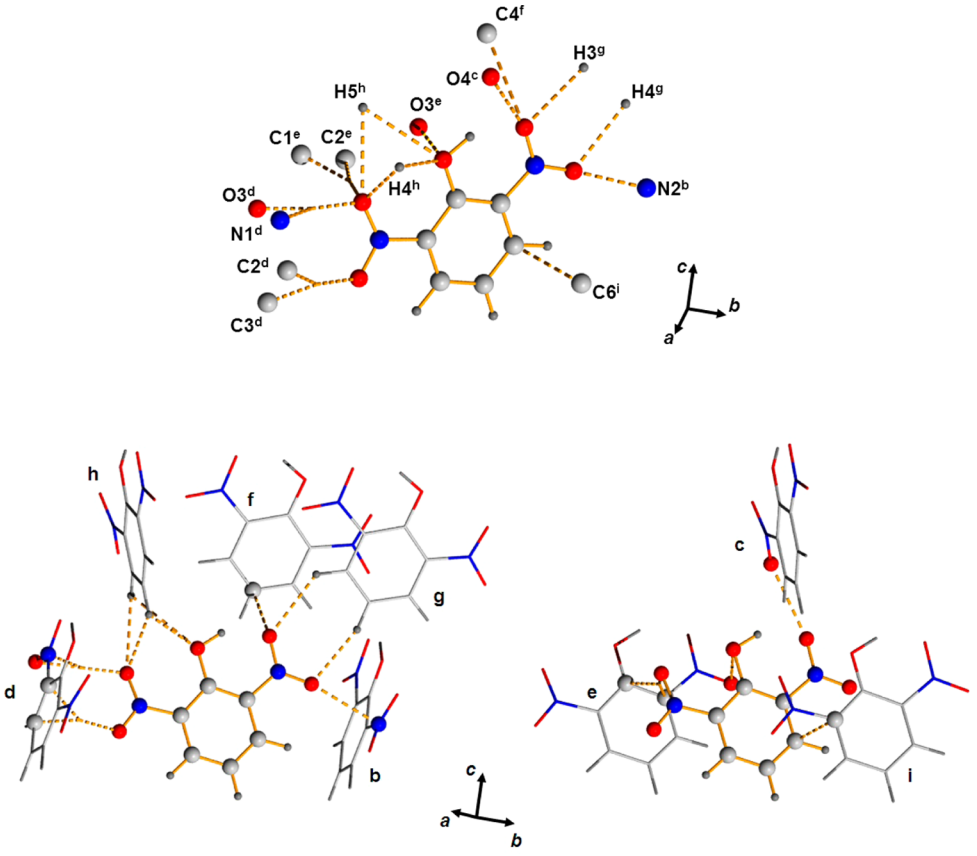

Figure 7. Upper view shows all intermolecular interactions to one molecule of DNP (see Table 3). Lower views show wire frame diagrams of the corresponding neighboring molecules (two sets for clarity to avoid overlaps). Roman numerals indicate the symmetry operators defined in Table 3.

directly to the N2 atom. It is a (3,+1) critical point instead that is aligned almost perfectly with the O3−N2 direction. Despite this being usually considered a "depletion" point, the Laplacian has a value as low as −53.16 eÅ^{-5}. Considering the oxygen atom alone, these findings comply with the polarized nature of the N−O bond, with electron density transferred from the bonding region to the oxygen atomic basin and accumulated in the nonbonding region and in particular in the lone pairs.

The Laplacian topology for N2 was also expected to be similar to that reported for urea. In both cases, the nitrogen atom can be considered as sp^2 hybridized, i.e., from an orbital point of view, being bonded to the three neighboring atoms with three sp^2 orbitals and the nonbonding p orbital hosting the remaining two of its five electrons. From a topological point of view, this would be highlighted by the presence of two NBM above and below the plane spanned by the sp^2 orbitals. As can be seen in Figure 6, this is not the case here, as instead of (3,−3) critical points we find three (3,−1) critical points placed at the vertices of a triangle and, as required by the topological relationship, a (3,+1) critical point between them. Again, all of them are characterized by a negative value of the Laplacian. Although at first surprising, we can rationalize this finding by observing that the (3,−1) critical points are actually saddle points linking the BM characterizing the N2−O4, N2−O5, and N2−C6 bonds. In the nitro group, the π interaction between the p orbitals of the N and O atoms is definitely enhanced compared to that observed between C and N in urea. While in the latter the nitrogen NBM are still present, in a nitro group the Laplacian topology of nitrogen is modified to account for the contribution to the bonds of the charge density "located" in the p orbital. The charge transfer is such that, on average, a value of the Laplacian of −17 eÅ^{-5} is found for the (3,−1) critical points (and −16 eÅ^{-5} for the (3,+1) critical point) compared to the reported −55 eÅ^{-5} for the NBM in urea. It is important to recognize that the results we find for the N2 atom is not a consequence of the crystal field as the same topology has been found for the optimized isolated molecule. In the crystal phase, when the O3···N2 interaction is formed, we can thus deduce that its geometry is related to the partial removal of charge density from the N p orbital (at 90° with respect to the plane of the nitro group) matching the partial removal of charge density from the region between the lone pairs of the oxygen atom.

Closely related to this is the π-stacking of the various DNP molecules. Although perfectly aligned along the *b* crystallographic axis, the rings are not perpendicular to this direction but are tilted by roughly 45°. As a result, the O4−N2−O5 nitro group is superimposed over the ring of the molecule beneath, and the overall stacking interactions are dominated by the O5···C1, O1···O3, and C3···C6 bonds (Figure 7). In the case of O5···C1, the bond path originating from O5 is pointing almost exactly at the midpoint of the C1−C2 bond. However, for the various models the positions of the bcp's are not identical, and these small differences (the distance between the two farthest bcp's is less than 0.2 Å) in their location may cause the bond path to terminate at a different nuclear attractor for the different models, in this case C1 for MM_{exp} and C2 for MM_{theo} and *theo* (marked † in Table 3). The same situation occurs for O5···N1 and O4···C3, although in this case the interactions take place between two molecules placed at 90° to each other.

DOI: 10.1021/cg5016725
Cryst. Growth Des. 2015, 15, 875−883

The intermolecular interactions are completed by a number of weak CH···O bonds (Table 3).

4. CONCLUSIONS

In this article, we have presented a quantitative charge density study of 2,6-dinitrophenol both from a highly accurate X-ray diffraction experiment and periodic ab initio calculations. The results obtained from the topological analysis of the multipole modeled densities agree quite well, the largest discrepancies being found for the Laplacian at the bcp of strong, heteroatom bonds.

In addition to the covalent bonds, the structure of this molecule in the solid state and in the gas phase was found to be largely dominated by a strong intramolecular O−H···O hydrogen bond and a weaker O···O closed shell interaction. Moderately strong N···O intermolecular interactions are consistent with the growth of the crystal along the *a* axis and the characteristic sawtooth-like chain that can be observed along this direction. Face-to-face stacking of the planar molecules is characterized by similar O···O, O···C, and C···C interactions.

■ ASSOCIATED CONTENT

Supporting Information

Crystallographic information file (CIF) including full multipole refinement for 2,6-dinitrophenol, normal probability plot and scale factor plot, fractal dimension plot, and observed and calculated structure factors. This material is available free of charge via the Internet at http://pubs.acs.org.

■ AUTHOR INFORMATION

Corresponding Author

*E-mail: a.pinkerton@utoledo.edu.

Notes

The authors declare no competing financial interest.

■ ACKNOWLEDGMENTS

We thank Dr. C. Gatti for providing a preliminary Windows version of TOPOND and for helpful discussions. This work was supported by the National Science Foundation (grant NSF-CHE-1213329).

■ REFERENCES

(1) Dunitz, J. D.; Gavezzotti, A. *Chem. Soc. Rev.* **2009**, *38*, 2622.
(2) Gilli, G.; Gilli, P. *J. Mol. Struct.* **2000**, *552*, 1.
(3) (a) Shishkina, A. V.; Zhurov, V. V.; Stash, A. I.; Vener, M. V.; Pinkerton, A. A.; Tsirelson, V. G. *Cryst. Growth Des.* **2013**, *13*, 816. (b) Zhurov, V. V.; Pinkerton, A. A. *Z. Anorg. Allg. Chem.* **2013**, *639*, 1969.
(4) Zhurov, V. V.; Zhurova, E. A.; Pinkerton, A. A. *J. Appl. Crystallogr.* **2008**, *41*, 340.
(5) Iwasaki, F.; Saito, M.; Aihara, A. *Acta Crystallogr., Sect. B* **1976**, *32*, 102.
(6) Tay, S. P.; Kraft, J.; Walker, S. *J. Phys. Chem.* **1976**, *80*, 303.
(7) Aakeröy, C. B. *Acta Crystallogr., Sect. B* **1997**, *53*, 569.
(8) Bader, R. F. W. Atoms in Molecules. *A Quantum Theory*; Oxford University Press: Oxford, UK, 1990.
(9) Espinosa, E.; Molins, E.; Lecomte, C. *Chem. Phys. Lett.* **1998**, *285*, 170.
(10) (a) Hardie, M. J.; Kirschbaum, K.; Martin, A.; Pinkerton, A. A. *J. Appl. Crystallogr.* **1988**, *31*, 815. (b) Kirschbaum, K.; Martin, A.; Parrish, D.; Pinkerton, A. A. *J. Phys.: Condens. Matter* **1999**, *11*, 4483.
(11) Otwinowski, Z.; Minor, W. *Methods Enzymol.* **1997**, *A276*, 307.
(12) Zhurova, E. A.; Zhurov, V. V.; Tanaka, K. *Acta Crystallogr., Sect. B* **1999**, *55*, 917.
(13) Blessing, R. H. *Acta Crystallogr., Sect. A* **1995**, *51*, 33. (b) Blessing, R. H. *J. Appl. Crystallogr.* **1997**, *30*, 421.
(14) Sheldrick, G. M. *Acta Crystallogr., Sect. A* **2008**, *64*, 112.
(15) Hansen, N. K.; Coppens, P. *Acta Crystallogr., Sect. A* **1978**, *34*, 909.
(16) Volkov, A.; Macchi, P.; Farrugia, L. J.; Gatti, C.; Mallison, P.; Richter, T.; Koritsanszky, T. *XD2006 − A Computer Program for Multipole Refinement, Topological Analysis of Charge Densities and Evaluation of Intermolecular Energies from Experimental or Theoretical Structure Factors*;2006.
(17) Stewart, R. F.; Davidson, E. R.; Simpson, W. T. *J. Chem. Phys.* **1965**, *42*, 3175.
(18) Allen, F. H. *Acta Crystallogr., Sect. B* **2002**, *58*, 380.
(19) (a) Dovesi, R.; Orlando, R.; Civalleri, B.; Roetti, C.; Saunders, V. R.; Zicovich-Wilson, C. M. *Z. Kristallogr.* **2005**, *220*, 571. (b) Dovesi, R.; Saunders, V. R.; Roetti, C.; Orlando, R.; C. M. Zicovich-Wilson, Pascale, F.; Civalleri, B.; Doll, K.; Harrison, N. M.; Bush, I. J.; D'Arco, P., Llunell, M. *CRYSTAL09 User's Manual*; University of Torino, Torino, Italy, 2009.
(20) (a) Becke, A. D. *J. Chem. Phys.* **1993**, *98*, 5648. (b) Lee, C.; Yang, W.; Parr, R. G. *Phys. Rev. B* **1988**, *37*, 785.
(21) Valenzano, L.; Torres, F. J.; Doll, K.; Pascale, F.; Zicovich-Wilson, C. M.; Dovesi, R. *Z. Phys. Chem.* **2006**, *220*, 893.
(22) Gatti, C. *TOPOND-98: An Electron Density Topological Program for Systems Periodic in N (N = 0−3) Dimensions. User's Manual*, CNR-ISTM, Milano, Italy, 1999.
(23) Zhurov, V. V.; Pinkerton, A. A. *Cryst. Growth Des.* **2014**, *14*, 5685.
(24) Stash, A.; Tsirelson, V. *J. Appl. Crystallogr.* **2002**, *35*, 371.
(25) Bader, R. F. W.; Slee, T. S.; Cremer, D.; Kraka, E. *J. Am. Chem. Soc.* **1983**, *105*, 5061.
(26) (a) Tsirelson, V. G.; Bartashevich, E. V.; Stash, A. I.; Potemkin, V. A. *Acta Crystallogr., Sect. B* **2007**, *63*, 142−150. (b) Bartashevich, E. V.; Nikulov, D. K.; Vener, M. V.; Tsirelson, V. G. *Comput. Theor. Chem.* **2011**, *973*, 33−39.
(27) Zhurova, E. A.; Tsirelson, V. G.; Stash, A. I.; Yakovlev, M. V.; Pinkerton, A. A. *J. Phys. Chem. B* **2004**, *108*, 20173.
(28) Espinosa, E.; Alkorta, I.; Elguero, J.; Molins, E. *J. Chem. Phys.* **2002**, *117*, 5529.
(29) We note that the estimation of interaction energies based on the critical point properties is really only valid for hydrogen bonds; hence, the values reported here should be considered qualitative.
(30) Chen, P. C.; Tzeng, S. C. *J. Mol. Struct.: THEOCHEM* **1999**, *467*, 243.
(31) Zhurov, V. V.; Zhurova, E. A.; Stash, A. I.; Pinkerton, A. A. *Acta Crystallogr., Sect. A* **2011**, *67*, 160.
(32) Gatti, C.; Saunders, V. R.; Roetti, C. *J. Chem. Phys.* **1994**, *101*, 10686.
(33) Brandenburg, K.; Putz, H. *Diamond: Crystal and Molecular Structure Visualization Crystal Impact*; http://www.crystalimpact.com/diamond.

DOI: 10.1021/cg5016725
Cryst. Growth Des. 2015, 15, 875−883